Sensors and Materials, Vol. 36, No. 8 (2024) 3395–3405
MYU Tokyo

S & M 3739

Temperature Dependence of Electrostatic Frequency Tunability of Ultrathin Si Nanoresonators

Wei Yu, Amit Banerjee,* Jun Hirotani, and Toshiyuki Tsuchiya

Department of Micro Engineering, Graduate School of Engineering, Kyoto University,
Kyoto Daigaku-Katsura C3, Nishikyo-ku, Kyoto 615-8540, Japan

(Received April 30, 2024; accepted July 8, 2024)

Keywords: NEMS resonators, resonance frequency, electrostatic tuning, temperature coefficient of frequency

Nanoresonators are crucial elements of various nano-electromechanical systems for the development of ultrasensitive sensing, efficient signal processing, biological detection, and so forth. Implementing methods that facilitate the wide tuning of the resonance frequency is beneficial for many of these applications. Ultrathin Si nanoresonators (width ~10 nm, length ~100 μm) can exhibit a wide electrostatic tunability of resonance frequency, which can be used for the easy electrostatic compensation of the thermal drift in resonance frequency among many other potential applications. How this tunability is impacted by temperature variation is a pertinent issue in many potential applications of tunable Si nanoresonators but currently remains unknown. In this study, we experimentally investigate the temperature dependence of the electrostatic tuning of a Si nanoresonator of ~80 nm width and ~200 μm length across a temperature range of 100–300 K. The results show significant decreases in electrostatic tuning range, efficiency, and resonance frequency tendency with decreasing temperature. We provide an approximate thermo-electromechanical model to describe this behavior and discuss how a dual tuning strategy by gate voltage and temperature can potentially bring further opportunities in terms of on-the-spot adjustment of the nanoresonator's frequency as demanded in specific applications.

1. Introduction

Nanomechanical resonators have emerged as crucial elements in various nano-electromechanical system (NEMS) applications, serving as the essential components for the development of ultrasensitive mass,[1] force,[2] and electric charge detection systems,[3] ultrafast and efficient communication methods,[4] next-generation computing devices,[5] and so forth. The efficient and often unprecedented performance of nanoresonators in many of these applications is attributed to their small mass and rich dynamic behavior.[6] Therefore, the degree to which the core dynamic characteristics of these nanoresonators, such as their resonance frequency (f_0), can be tuned plays a vital role in enhancing their functionality, ensuring stability, bringing operation

*Corresponding author: e-mail: banerjee.amit.3v@kyoto-u.ac.jp
https://doi.org/10.18494/SAM5096

ISSN 0914-4935
https://myukk.org/

flexibility and versatility, and so forth.[6] Achieving practicable means to attain significant resonance frequency tunability at the application stage of nanoresonators promises potential benefits for numerous practical applications, such as improving the nanoresonator-based sensor's responsivity,[7] developing filters with adjustable bandwidths,[8] mode matching in inertial sensors,[9] enhancing the efficiency of mechanical energy-harvesting devices,[10] impedance matching in nanoelectronic circuits,[11] and developing precise NEMS timing devices.[12] A common strategy for tuning the resonance frequency of nanoresonators is by employing various physical mechanisms, such as mechanical stress,[13,14] electrostatic force,[15] and thermal and electrothermal effects to manipulate the axial strain on nanoresonators.[16,17] A common theme in these tuning mechanisms is attributed to the fact that nanoresonators' natural frequencies are strongly affected by the axial strain, unlike their micrometer-scale counterparts where the natural frequency is predominantly governed by elastic stiffness determined by the material and geometry. Thus, in post-fabricated devices, mechanisms capable of manipulating the axial strain on nanoresonators provide easy access to resonance frequency tuning. For instance, Ning *et al.* demonstrated the tuning of resonance frequency of their carbon nanotube nanoresonators using a piezoelectric substrate to exert an axial strain.[13] The resonance frequency can be tuned 20 times in this way. Similarly, Truax *et al.* reported a mechanical strain modification strategy that involves using a MEMS electrothermal actuator to apply in-plane tension to a carbon nanotube resonator, which resulted in an increase in resonance frequency from 10 to 60 MHz.[14] Additionally, the application of electrostatic force has been shown to effectively tune the resonance frequency of graphene NEMS resonators by up to 58%, which is performed by varying the DC gate voltage V_g between the resonator and a nearby gate electrode.[15] In other studies, the resonance frequencies of MoS_2 and graphene resonators have also been shown to be tunable by varying the thermal pulse[16] or temperature.[17]

The ultrawide tunability of resonance frequency is predominantly achieved in atomically thin material-based resonators, which are notably sensitive to strain variations owing to their extreme aspect ratio that leads to a negligible elastic stiffness. The resonance frequency tuning ranges (T_R) exceeding 100% have been reported using purely electrostatic forces at room temperature in graphene,[18] black phosphorus,[19] and MoS_2 resonators.[20] In a recent work, we have demonstrated that a comparable room-temperature electrostatic frequency tunability is also achievable in monolithically fabricated ultrathin Si nanoresonators.[21] To demonstrate this, we developed a top-down fabrication method to create 20–300-nm-wide and 100–300-μm-long Si nanoresonators. In one of our Si nanoresonators with a width of ~40 nm and a length of ~200 μm (height ~7.5 μm), we achieved a tuning range of ~70% of initial frequency at the average tuning efficiency T_e of ~7% V^{-1}.[21] These ultrathin Si nanoresonator devices are fabricated from a standard, commercially purchased silicon-on-insulator (SOI) wafer using a standardized cleanroom Si microfabrication process [Fig. 1(A)]. The developed fabrication process simultaneously fabricates all device components, namely, the nanoresonators and in-plane, parallel side gates for the electrostatic actuation and capacitive detection of the nanoresonators' motion [Fig. 1(B)]. Achieving such a high tunability in nanoresonators fabricated using conventional SOI materials and by established microfabrication processes can lead to the rapid development of a scalable fabrication process for tunable nanoresonators. In addition, since our

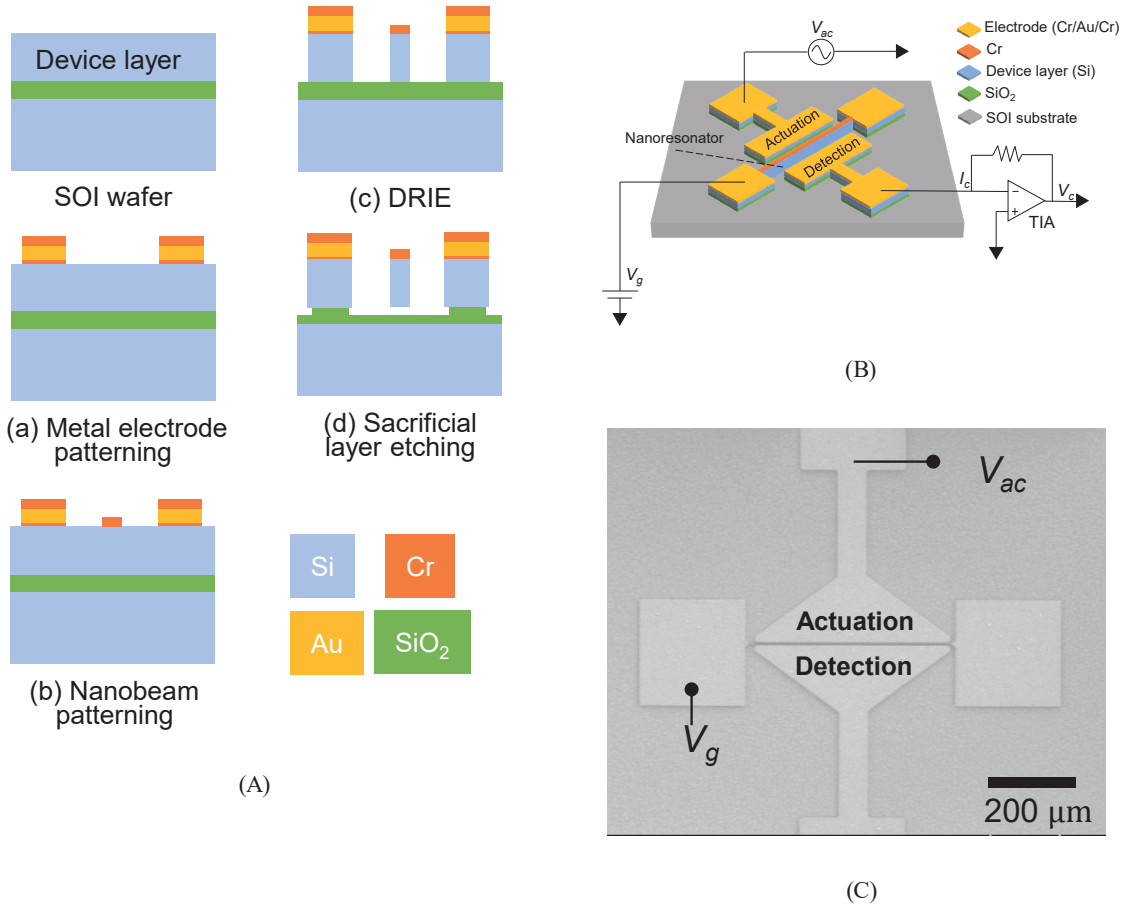

Fig. 1. (Color online) Fabrication, geometry, and characterization setup of the developed ultrathin silicon nanoresonator. (A) Fabrication of developed ultrathin Si NEMS resonator devices. (B) Schematic illustration of the device structure and actuation/read-out circuits. (C) SEM image of a device.

nanoresonators and their substrates are both made from the same material (Si), our ultrathin nanoresonators show a relatively smaller temperature coefficient of frequency (TCF),[21] promising a lesser drift in resonance frequency due to temperature fluctuation. This can potentially lead to a higher frequency stability and an efficient drift compensation by electrostatic tuning. However, in such ultrathin nanoresonator devices, the electrostatic tuning efficiency itself is expected to be significantly affected by temperature variation, as reported in various atomically thin resonators, where the resonance frequency tunability typically decreases when temperature decreases.[17] A quantitative experimental investigation of the temperature dependence of this electrostatic tunability of resonance frequency of Si nanoresonators can provide (a) means to control the electrostatic tuning efficiency by substrate temperature control and (b) insight into the efficacy and limitations of the electrostatic compensation of thermal-fluctuation-induced frequency drift. In this work, we report a detailed experimental investigation on the temperature dependence of the electrostatic resonance frequency tuning behavior of ultrathin Si nanoresonators with a width of ~80 nm, a length of ~200 µm, and a height of 7.5 µm

between room temperature (~300 K) and 100 K. We observed that the frequency tuning range, efficiency, and tuning trend (upward versus downward shift in frequency with an increase in gate voltage) strongly depend on the substrate temperature. The tuning range for an identical V_g (10–20 V) range was observed to steadily decline as the nanoresonator temperature was reduced. Moreover, the tuning trend was also observed to vary with temperature, viz., with increasing V_g, a strictly upward frequency tuning was observed at room temperature, while a non-monotonic trend emerged as the temperature was reduced. We explain these behaviors using an approximate thermo-electromechanical model of the Si nanoresonator device. We believe that the results of this study will contribute to the development of scalable, tunable, and stable Si nanoresonators for various applications.

2. Device Fabrication and Characterization

The Si nanoresonator device fabricated for this study is composed of a straight, double-clamped Si nanostructure with a rectangular cross section, an electrostatic actuation electrode, and a capacitive detection electrode [Fig. 1(B)]. As schematically depicted in Fig. 1(A), the fabrication of our silicon nanomechanical resonators started from a SOI wafer with a 7.5-μm-thick n-type single-crystal (100) silicon device layer (dopant: As, ~3×10^{19} cm^{-3}; resistivity ~0.002 Ω.cm). The sacrificial layer was made of a ~2-μm-thick SiO_2 film and the handle layer was made of a 508 ± 5-μm-thick Si film. Following wafer cleaning and the removal of the native oxide from the top of the device layer, the actuation and detection electrodes were patterned by UV lithography (Union PEM-800, double-sided aligner), Cr/Au/Cr metal thin-film (thicknesses of 10/70/50 nm, respectively) deposition, and a lift-off process. Subsequently, electron beam lithography (ELS-F130HM, Elionix) was employed to pattern the ultrathin nanoscale resonator structure, and a Cr film (50 nm) pattern of the nanoresonator was achieved after the lift-off process. The device layer Si was then etched by deep reactive-ion etching (Bosch process, Samco, RIE-800iPB-KU), and the nanoresonator structure was suspended by vapor hydrofluoric (HF) acid etching (Sumitomo Precision Products, MLT-SLE-Ox), which selectively removes the underlying sacrificial SiO_2 layer. This vapor phase chemical etching process can prevent the stiction of the suspended nanoresonator with nearby structures such as the gate electrodes and the handle layer. Further details of the fabrication steps, recipes, and so forth are provided elsewhere.[21] By this fabrication process, nanoresonators with lengths (L) between 100 and 300 μm, widths (t) from 20 to 300 nm, heights of ~7.5 μm (determined by the device layer thickness), and gap distances (g_0) between the nanoresonator and the actuation and the detection electrode from 1 to 3 μm were successfully fabricated, as we reported in our previous study on their room-temperature electrostatic tunability.[21] An SEM image of a Si nanoresonator device is shown in Fig. 1(C).

For the dynamic characterization of our Si nanoresonators, DC bias voltage (V_g) was applied (Agilent, E3647A) to one of the nanoresonators' anchors via the metal thin film on top of it. The DC and AC (V_{ac}) voltages applied between the beam and the electrostatic actuator periodically actuated the nanoresonators at the AC voltage's angular frequency. This oscillation induces capacitance fluctuations between the beam and the detection electrode, generating a periodic

current signal (I_c) for electrical read-out. This signal was amplified and converted to a voltage output (V_c) through a transimpedance amplifier (TIA) and analyzed using a lock-in amplifier (Zurich Instruments MFLI 500 kHz/5 MHz). When the frequency of the applied drive voltage approached the resonator's resonance frequency of its fundamental flexural mode vibration, the amplitude of vibration of the beam and, consequently, the read-out signal of the device reached their maximum values; thus, the resonance response can be detected by frequency sweep around this frequency. All measurements were conducted within a high-vacuum environment (~1.1×10^{-4} Pa) in a vacuum probe station equipped with a substrate temperature control facility, which was achieved by cooling the sample stage via liquid nitrogen and varying the stage temperature with a stage heater that automatically stabilizes the temperature at a set point.

3. Results and Discussion

3.1 Temperature effect on electrostatic tuning

A nanoresonator device of 80 nm width and 200 μm length was chosen for the investigation of the electrostatic resonance frequency tuning behavior at various temperatures within the vacuum chamber. The substrate temperature in the vacuum chamber was reduced from room temperature (~300 K) to 100 K at intervals of 50 K. At each temperature, the nanoresonator's frequency responses were measured in its linear response regime with a constant AC drive voltage of 1 mV, while V_g was varied from 10 to 20 V. Figure 2(a) shows the detected frequency response at 300 and 200 K. At both temperatures, an increase in resonance frequency was observed with increasing V_g, indicating an upward electrostatic frequency tunability. This upward resonance frequency tuning with increasing V_g is attributed to a static deflection of the

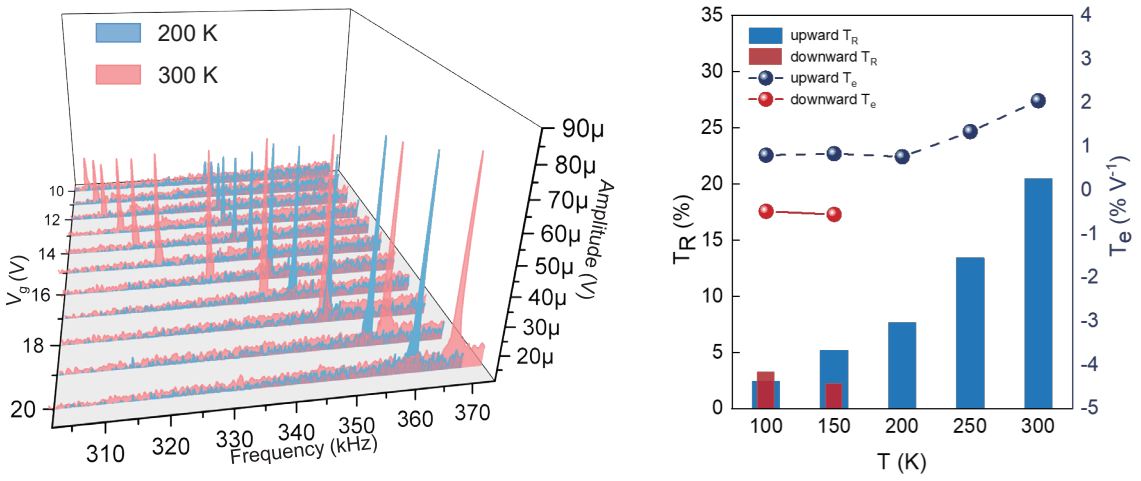

(a) (b)

Fig. 2. (Color online) (a) Experimental results of resonance response detected from a device with length of 200 μm and width of 80 nm as gate voltage (V_g) varies from 10 to 20 V at substrate temperatures of 300 and 200 K. (b) Measured resonance frequency tuning range (T_R) (bar chart), alongside tuning efficiency (T_e) (dot-line chart), where T_e is calculated as T_R divided by the applied voltage range. The upward and downward tuning conditions are separately presented.

nanoresonator due to the applied electrostatic force, which increases the axial strain of the nanoresonator.[21] The significant role of the axial strain on the resonance frequency was appreciable even at the lowest V_g (10 V) since the measured frequency (f_0) was ~17.3 times (under the 300 K condition) and 19.1 times (under the 200 K condition) higher than what would be expected from an equivalent tension-free Euler–Bernoulli beam.[22] In the plot of Fig. 2(a), notably, at 200 K, a higher f_0 at V_g of 10 V and a lower f_0 at 20 V were recorded compared with the observation made at 300 K, indicating an increased initial resonance frequency (f_0 at V_g = 10 V) and a narrower electrostatic tuning range and a lower tuning efficiency. To quantify such measurements, we define thve tuning range for both upward tuning and downward tuning trends, where the upward tuning range $T_{R\text{-}upward}$ is given by $T_{R\text{-}upward} = \left(f_u^{max} - f_0^{min} \right) / f_0^{min} \times 100\%$, where f_0^{min} and f_u^{max} are the minimum and upward-tuned maximum resonance frequencies, respectively, measured within a V_g range of 10–20 V. Similarly, the downward tuning range $T_{R\text{-}downward}$ is defined as $T_{R\text{-}downward} = \left(f_d^{max} - f_0^{min} \right) / f_d^{max} \times 100\,\%$, where f_d^{max} is the maximum resonance frequency during downward tuning. We also define the local tuning efficiency T_e for both tuning trends, which is the ratio of the tuning range, either upward ($T_{R\text{-}upward}$) or downward ($T_{R\text{-}upward}$), to the voltages required for the respective tuning.

In Fig. 2(a), the measured T_R achieved diminished from 20.5% at 300 K to 7.5% at 200 K. The bar plot in Fig. 2(b) shows the measured resonance frequency tuning range, and the circle-dash line plot shows the corresponding tuning efficiency T_e as V_g was varied between 10 and 20 V across different substrate temperatures. Note that the frequency tuning trend can be non-monotonic, viz., the minimum frequency is observed at an intermediate value of V_g [Fig. 3(a)].[21] In such a scenario, with increasing V_g, one part of the tuning data will show a downward frequency tuning trend, while the other part will show an upward frequency tuning trend. In the plot of Fig. 2(b), the downward trends are indicated by red bars in the plot, while the upward frequency trends are indicated by blue bars. A consistent decrease in T_R was observed with the reduction in temperature below 300 K. The downward tuning trend was observed at temperatures of 150 and 100 K. The upward T_e decreased from 300 to 200 K and remained at relatively low values in the range from 200 to 100 K. The downward T_e showed a certain increase when the temperature changed from 150 to 100 K.

The results of the electrostatic tuning of resonance frequency conducted at various temperatures are shown in the plot of Fig. 3(a). Beside the reduction in T_R as mentioned above, a non-monotonic trend in tuning emerged at a lower temperature. The downward trend in frequency tuning signifies a dominant role of the electrostatic softening effect[23] over the deflection-induced stretching of the nanoresonator, leading to an overall downward tuning of the resonance frequency. The competition between these two mechanisms can be understood using an approximate electromechanical model of the nanoresonator,[21] which can approximately predict the resonance frequency.

$$f_0\left(V_g, T\right) = \frac{1}{2\pi}\sqrt{\left(J_2\frac{Et^2}{6\rho L^4} + J_1\frac{2E\varepsilon\left(T\right)}{\rho L^2}\right) - \left(\frac{o_2\zeta\epsilon_0}{\rho t g_0^3}V_g^2\right) + \left(\frac{3o_1^2\zeta^2\epsilon_0^2}{4\rho g_0^4 E t^2 \varepsilon^2\left(T\right)}V_g^4\right)} \qquad (1)$$

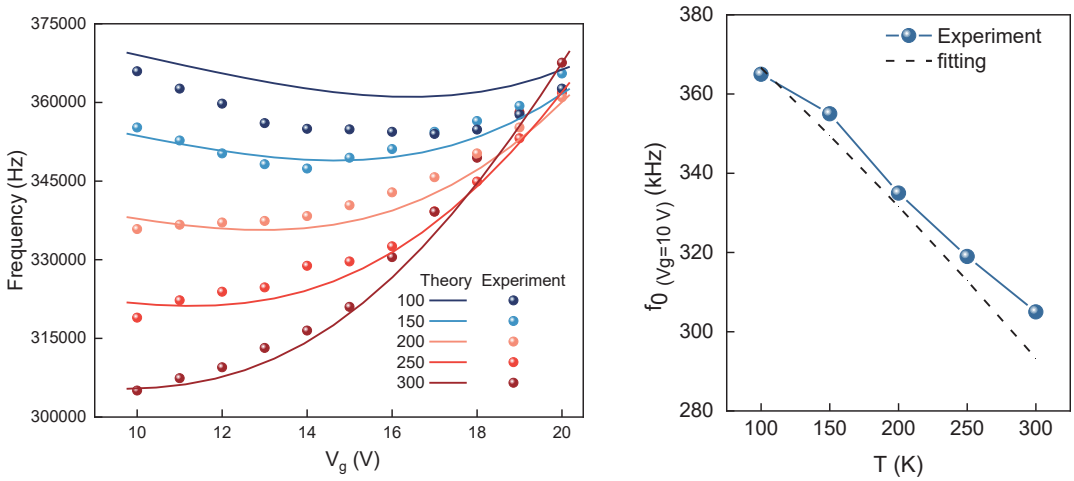

(a) (b)

Fig. 3. (Color online) (a) Estimated resonance frequency tuned by gate voltage during the device's temperature decrease from 300 to 100 K based on the approximate tuning model expressed in Eq. (1) with the experimentally measured results. (b) Experimental frequency data at V_g= 10 V fitted with the theoretically expected frequency value assuming a thermal expansion coefficient difference (Δa_{th}) of ~1.3 × 10^{-6} K^{-1} between the nanoresonator and the substrate.

Here, E is Young's modulus, ρ is the density of the silicon, $\varepsilon(T)$ is the axial tensile strain at V_g = 0 V and at a given temperature (T), ϵ_0 is the permittivity of free space, $\zeta \approx 1$ is a capacitance correction factor, and J_i (i = 1, 2) and o_j (j = 1, 2) are dimensionless constants derived from the appropriate deflection-shape function. In this study, $J_1 = 5.3$, $J_2 = 64.0$, $o_1 = 0.67$, and $o_2 = 0.53$ are used on the basis of the parabolic function deflection shape.[21] The first term under the square-root symbol in Eq. (1) represents the initial resonance frequency without the effect of V_g, predominantly affected by $\varepsilon(T)$. The second term indicates the decrease in f_0, which is contributed by the electrostatic softening effect, and the final term indicates the stretching effect. The actual frequency tuning trend is determined by the competition between these last two terms, while the initial frequency increases with $\varepsilon(T)$. The condition for the upward tuning frequency is shown in Eq. (2), which indicates that in the case of an increase in axial strain, a higher V_g is required to exhibit an upward frequency tuning trend.

$$\left|V_g\right| \geq \sqrt{\frac{2o_2 g_0 Et}{3o_1^2 \zeta \epsilon_0}} \varepsilon(T) \tag{2}$$

The axial strain $\varepsilon(T)$ in the nanoresonator is modeled by a difference in thermal expansion coefficient (Δa_{th}) between the material of the nanoresonator (Si) and that of the substrate (SiO_2/Si), which can be written as[24]

$$\varepsilon(T) = \varepsilon_0(T_0) + \Delta a_{th}(T - T_0), \tag{3}$$

where ε_0 is the axial tensile strain at a reference temperature (T_0). In Fig. 3(b), we plot $f_0\left(V_g = 10\text{ V}\right)$ measured at different temperatures. We fit this trend using Eqs. (1) and (3) to extract the values of Δa_{th} ~1.3 × 10^{-6} K^{-1} and ε_0 (300 K) ~23 MPa. Note that the increase in $f_0\left(V_g = 10\text{ V}\right)$ with decreasing temperature suggests an increase in $\varepsilon\left(T\right)$ in the resonator. This explains the tuning trend variation [Fig. 3(a)], which goes from upward at higher temperatures (T = 300, 250, and 200 K) to non-monotonic at lower temperatures (T = 150 and 100 K). Using the fitting parameters extracted from Fig. 3(b), we fit the resonance frequency tuning data in Fig. 3(a).

3.2 Tunable temperature coefficients of frequency

The results shown in Figs. 2 and 3 reveal the temperature dependence of the electrostatic tunability of resonance frequency in an ultrathin Si nanoresonator between 100 and 300 K, where a strong relationship between temperature and tunability is observed. The results not only indicate significant decreases in tuning ranges and tuning efficiencies but also show a more complex behavior in terms of the frequency tuning trend, suggesting that the stage temperature control can be a potential method to control the electrostatic tunability. Thus, a dual tuning strategy of the nanoresonator by V_g and T can provide further opportunities in terms of on-the-spot adjustment of the nanoresonator's frequency as demanded in specific applications.

Another noteworthy observation from Fig. 3 is that the span of resonance frequencies across the temperature range (100–300 K) shrinks with increasing V_g. The resonance frequency span indicates the temperature-fluctuation-induced variability in the resonance frequency (thermal drift) of the device during operation, which is a critical factor in the design and performance of resonator devices used in telecommunications, navigation, and timekeeping.[25] A wider frequency span suggests a higher sensitivity to temperature fluctuations, whereas a smaller span indicates a higher temperature stability. Note that the higher temperature sensitivity of the resonance frequency of the device is not always undesirable; in applications such as resonator-based temperature sensors, it can be advantageous. Compared with MEMS resonators, NEMS resonators typically exhibit a higher sensitivity to temperature fluctuation because they are more susceptible to strain change, making them well suited for temperature sensing but less desirable in applications where frequency stability is important (such as in timing devices). The temperature coefficient of frequency (TCF) defined as the relative resonance frequency shift per degree Kelvin of temperature change is commonly used for evaluating such temperature sensitivity. In recent reports, the TCFs of conventional NEMS resonators, such as the MoS_2 and h-BN resonators, are around −3960[26] and −2850 ppm/K,[27] respectively. For graphene resonators, TFC is much higher, which can reach around −8600 ppm/K.[18] In contrast, conventional MEMS resonators exhibit typical TCFs in the range from −20 to −100 ppm/K.[28,29]

The measured device's TCFs at different V_g values were estimated by calculating the resonance frequency shift per degree Kelvin as the temperature decreased from 300 to 250, 200, 150, and 100 K, as shown in Fig. 4. Initially, TCF exhibited negative values and increased with V_g, and it subsequently exhibited positive values. The lowest observed absolute TCF was approximately 3.6 ppm/K at V_g of 17 V, comparable to those of conventional MEMS resonators,

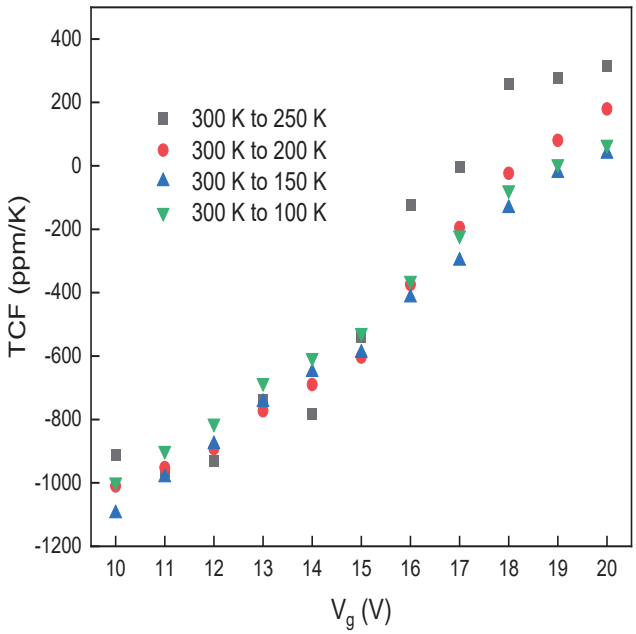

Fig. 4. (Color online) The measured TCFs calculated in different temperature variation ranges change with the increase in V_g.

while the initial TCF with V_g = 10 V was around −1096 ppm/K, aligning with those of typical NEMS resonators. Both the value and sign of TCF can be tuned by adjusting V_g, which indicates that the direction of frequency shift relative to the temperature variation can also be tuned. A positive TCF implies that the frequency increases with temperature, whereas a negative TCF suggests a decrease in frequency as temperature increases. These results demonstrate that the proposed gate-voltage-controlled method effectively adjusts the resonators' temperature sensitivity, enabling the dual functions of temperature sensing and temperature stability within the same device.

Note that although the proposed stage temperature control method while effective in laboratory settings may pose significant challenges in practical applications, where attaining a stable, cryogenic temperature may be difficult owing to cost or design limitations. The relatively high TCF in our nanoresonators compared with conventional MEMS resonators can pose a challenge in applications requiring high frequency stability such as in timing applications. Fortunately, the ultrawide electrostatic frequency tunability achievable at room temperature in our devices can potentially provide an efficient and easy frequency drift compensation for the native stress ($E\varepsilon_0(T_0)$) on the nanoresonators, i.e., stress not attributed to electrostatic force, introduced during device fabrication and packaging is kept reasonably low. Thus, some consideration regarding this point should be given during the design, fabrication, and packaging of the devices. Since, TCF and thus the frequency stability of the nanoresonator depend on the thermal expansion coefficient mismatch between the materials of the nanoresonator and that of the substrate (SiO_2/Si), a potential method to optimize the TCF will be to adjust the thickness of the sacrificial SiO_2 layer within the limitations of the fabrication and detection processes, which would require further experimental exploration in the future.

4. Conclusions

In this study, we explored the resonance frequency tuning of an ultrathin Si NEMS resonator of ~80 nm width and ~200 μm length, focusing on the interplay between the electrostatic and temperature tuning of resonance frequency. We revealed that the electrostatic resonance frequency tuning range consistently narrows as temperature decreases from 300 to 100 K, suggesting that temperature control could serve as a potential method for controlling the electrostatic tunability. This behavior is primarily attributed to the axial strain variation induced by the differential thermal expansion of the materials of the nanoresonator and its substrate. Furthermore, by manipulating the gate voltage, the temperature sensitivity of the device can be precisely controlled. This capability enables the dual functionality of the resonators to act both as highly sensitive temperature sensors and as devices exhibiting high temperature stability. Currently, this study has concentrated on the process of cooling the developed ultrathin silicon nanoresonators. Future research will extend to exploring frequency tuning behavior during heating, broadening our understanding of the frequency tuning of ultrathin silicon nanoresonators.

Acknowledgments

This work was supported by the Japan Society for the Promotion of Science (JSPS) Grants-in-Aid for Scientific Research (JSPS KAKENHI Grant Number JP21K14513), The Kyoto University Research Fund for Young Scientists (Start-Up) FY 2020, and JST SPRING Grant Number JPMJSP2110. Part of this work was supported by the "Advanced Research Infrastructure for Materials and Nanotechnology in Japan (ARIM)" of the Ministry of Education, Culture, Sports, Science and Technology (MEXT) (Grant Number JPMXP1222KT1420). We acknowledge technical support from the Nanotechnology Hub in Kyoto University.

Conflict of Interest

The authors declare that they have no conflict of interest.

References

1 J. Chaste, A. Eichler, J. Moser, G. Ceballo, R. Rurali, and A. Bachtold: Nat. Nanotechnol. **7** (2012) 301. https://doi.org/10.1038/nnano.2012.42
2 J. Moser, J. Güttinger, A. Eichler, M. J. Esplandiu, D. E. Liu, M. I. Dykman, and A. Bachtold: Nat. Nanotechnol. **8** (2013) 493. https://doi.org/10.1038/nnano.2013.97
3 X. Wang, X. Wei, D. Pu, and R. Huan: Microsyst. Nanoeng. **6** (2020) 78. https://doi.org/10.1038/s41378-020-00192-4
4 A. Erbe and R. H. Blick: IEEE Trans. Ultrason. Ferroelectr. Freq. Control **49** (2002) 1114. https://doi.org/10.1109/TUFFC.2002.1026023
5 S. Rips and M. J. Hartmann: Phys. Rev. Lett. **110** (2013) 120503. https://doi.org/10.1103/PhysRevLett.110.120503
6 B. Xu, P. Zhang, J. Zhu, Z. Liu, A. Eichler, X.-Q. Zheng, J. Lee, A. Dash, S. More, S. Wu, Y. Wang, H. Jia, A. Naik, A. Bachtold, R. Yang, P. X.-L. Feng, and Z. Wang: ACS Nano **16** (2022) 15545. https://doi.org/10.1021/acsnano.2c01673

7 W. Yu, A. Banerjee, J. Hirotani, and T. Tsuchiya: Jpn. J. Appl. Phys. **63** (2024) 03SP74. https://doi.org/10.35848/1347-4065/ad2979
8 G. Chaudhary, Y. Jeong, and J. Lim: IEEE Trans. Microw. Theory Tech. **61** (2013) 107. https://doi.org/10.1109/TMTT.2012.2222910
9 A. Eichler, M. del Álamo Ruiz, J. A. Plaza, and A. Bachtold: Phys. Rev. Lett. **109** (2012) 025503. https://doi.org/10.1103/PhysRevLett.109.025503
10 C. Peters, D. Maurath, W. Schock, F. Mezger, and Y. Manoli: J. Micromech. Microeng. **19** (2009) 094004. https://doi.org/10.1088/0960-1317/19/9/094004
11 C. Chen, S. Lee, V. V. Deshpande, G.-H. Lee, M. Lekas, K. Shepard, and J. Hone: Nat. Nanotechnol. **8** (2013) 923. https://doi.org/10.1038/nnano.2013.232
12 SiTime. XCalibur™ active resonators. https://www.sitime.com/products/resonators (accessed April 2024)
13 Z. Y. Ning, T. W. Shi, M. Q. Fu, Y. Guo, X. L. Wei, S. Gao, and Q. Chen: Nano Lett. **14** (2014) 1221. https://doi.org/10.1021/nl4040913
14 S. Truax, S.-W. Lee, M. Muoth, and C. Hierold: Nano Lett. **14** (2014) 6092. https://doi.org/10.1021/nl501853w
15 R. A. Barton, I. R. Storch, V. P. Adiga, R. Sakakibara, B. R. Cipriany, B. Ilic, S.P. Wang, P. Ong, P. L. McEuen, J. M. Parpia, and H. G. Craighead: Nano Lett. **12** (2012) 4681. https://doi.org/10.1021/nl302036x
16 Z. Wang, R. Yang, and P. X.-L. Feng: Nanoscale **13** (2021) 18089. https://doi.org/10.1039/D1NR03286K
17 C. Chen, S. Rosenblatt, K. I. Bolotin, W. Kalb, P. Kim, I. Kymissis, H. L. Stormer, T. F. Heinz, and J. Hone: Nat. Nanotechnol. **4** (2009) 861. https://doi.org/10.1038/nnano.2009.267
18 A. M. V. D. Zande, R. A. Barton, J. S. Alden, C. S. Ruiz-Vargas, W. S. Whitney, P. H. Q. Pham, J. Park, J. M. Parpia, H. G. Craighead, and P. L. McEuen: Nano Lett. **10** (2010) 4869. https://doi.org/10.1021/nl102713c
19 H. Jia, Z. Wang, and P. Feng: Proc. 2016 Solid-State Sensors, Actuators and Microsystems Workshop (Hiltonhead 2016) 416.
20 P. Prasad, N. Arora, and A. K. Naik: Nano Lett. **19** (2019) 5862. https://doi.org/10.1021/acs.nanolett.9b01219
21 W. Yu, Y. Ohara, C. Meffan, J. Hirotani, A. Banerjee, T. Tsuchiya: Nano Lett. **23** (2023) 11517. https://doi.org/10.1021/acs.nanolett.3c03164
22 S. Schmid, L. G. Villanueva, and M. L. Roukes: Fundamentals of Nanomechanical Resonators (Springer, Berlin, 2016) p. 6.
23 J. Lee, Z. Wang, K. He, R. Yang, J. Shan, and P. X.-L. Feng: Sci. Adv. **4** (2018) eaao6653. https://doi.org/10.1126/sciadv.aao6653
24 I. Voiculescu and M. Zaghloul: Nanocantilever Beams: Modeling, Fabrication, and Applications (Jenny Stanford, New York, 2015) Part. 3.
25 G. Wu, J. Xu, E. J. Ng, and W. Chen: J. Microelectromechanical Syst. **29** (2020) 1137. https://doi.org/10.1109/JMEMS.2020.3020787
26 R. Yang, Z. Wang, and P. X.-L. Feng: Proc. 2015 Joint Conf. IEEE Int. Frequency Control Symp. & the European Frequency and Time Forum (IEEE, 2015) 198. https://doi.org/10.1109/FCS.2015.7138822
27 X.-Q. Zheng, J. Lee, and P. X.-L. Feng: Microsyst. Nanoeng. **3** (2017) 17038. https://doi.org/10.1038/micronano.2017.38
28 S. Wang, W. Chen, B. Bahr, W. Fang, S. Li, and D. Weinstein: IEEE Trans. Ultrason. Ferroelectr. Freq. Control **62** (2015) 1166. https://doi.org/10.1109/TUFFC.2014.006724
29 X. Li, J. Liang, H. Zhang, X. Yang, H. Zhang, W. Pang, and M. Zhang: Appl. Phys. Lett. **110** (2017) 263502. https://doi.org/10.1063/1.4990285